Enhanced electrical and magnetic properties in La0.7Sr0.3MnO3 thin films deposited on CaTiO3-buffered silicon substrates

C. Adamo, L. Méchin, T. Heeg, M. Katz, S. Mercone, B. Guillet, S. Wu, J.-M. Routoure, J. Schubert, W. Zander, R. Misra, P. Schiffer, X. Q. Pan, and D. G. Schlom

Citation: APL Materials **3**, 062504 (2015); doi: 10.1063/1.4915486
View online: http://dx.doi.org/10.1063/1.4915486
View Table of Contents: http://scitation.aip.org/content/aip/journal/aplmater/3/6?ver=pdfcov
Published by the AIP Publishing

Enhanced electrical and magnetic properties in $La_{0.7}Sr_{0.3}MnO_3$ thin films deposited on $CaTiO_3$-buffered silicon substrates

C. Adamo,[1,2] L. Méchin,[3] T. Heeg,[1] M. Katz,[4] S. Mercone,[5] B. Guillet,[3] S. Wu,[3] J.-M. Routoure,[3] J. Schubert,[6] W. Zander,[6] R. Misra,[7] P. Schiffer,[7,8] X. Q. Pan,[4] and D. G. Schlom[1,9,a]

[1]*Department of Materials Science and Engineering, Cornell University, Ithaca, New York 14853-1501, USA*
[2]*Department of Applied Physics, Stanford University, Stanford, California 94305, USA*
[3]*Groupe de Recherche en Informatique, Image, Automatique et Instrumentation de Caen, (GREYC-UMR 6072), CNRS-ENSICAEN—Université de Caen Basse-Normandie, 6 Boulevard Maréchal Juin, 14050 Caen Cedex, France*
[4]*Department of Materials Science and Engineering, University of Michigan, Ann Arbor, Michigan 48109, USA*
[5]*Laboratoire de Sciences des Procédés et des Matériaux, UPR3407, CNRS, Institut Galilee, Universite Paris-Nord, Villetaneuse, France*
[6]*Peter Grünberg Institute (PGI9-IT), JARA-Fundamentals of Future Information Technology, Research Centre Jülich, Jülich D-52425, Germany*
[7]*Department of Physics and Materials Research Institute, The Pennsylvania State University, University Park, Pennsylvania 16802, USA*
[8]*Department of Physics, University of Illinois at Urbana-Champaign, Urbana, Illinois 61801, USA*
[9]*Kavli Institute at Cornell for Nanoscale Science, Cornell University, Ithaca, New York 14853-1501, USA*

(Received 24 January 2015; accepted 26 February 2015; published online 24 April 2015)

We investigate the suitability of an epitaxial $CaTiO_3$ buffer layer deposited onto (100) Si by reactive molecular-beam epitaxy (MBE) for the epitaxial integration of the colossal magnetoresistive material $La_{0.7}Sr_{0.3}MnO_3$ with silicon. The magnetic and electrical properties of $La_{0.7}Sr_{0.3}MnO_3$ films deposited by MBE on $CaTiO_3$-buffered silicon ($CaTiO_3$/Si) are compared with those deposited on $SrTiO_3$-buffered silicon ($SrTiO_3$/Si). In addition to possessing a higher Curie temperature and a higher metal-to-insulator transition temperature, the electrical resistivity and $1/f$ noise level at 300 K are reduced by a factor of two in the heterostructure with the $CaTiO_3$ buffer layer. These results are relevant to device applications of $La_{0.7}Sr_{0.3}MnO_3$ thin films on silicon substrates. [http://dx.doi.org/10.1063/1.4915486]

The full spectrum of electronic, optical, and magnetic properties—e.g., insulating, semiconducting, superconducting, ferroelectric, and ferromagnetic effects—is found within the structurally compatible family of perovskite oxides. The integration of these epitaxial functional oxides with silicon substrates offers significant opportunities for applications.[1–8] Among them are micro-electromechanical systems (MEMS) based on epitaxial piezoelectric layers[9–13] and suspended bolometers based on epitaxial $La_{0.7}Sr_{0.3}MnO_3$ thin films.[14] The use of silicon substrates greatly facilitates the fabrication of MEMS and suspended bolometers, where three-dimensional structures can be efficiently realized by volume silicon micromachining using conventional techniques such as isotropic etching in alkaline solutions (KOH, TMAH, etc.) or reactive ion etching.[15,16] The ideal case

[a]Author to whom correspondence should be addressed. Electronic mail: schlom@cornell.edu

for such silicon-based heterostructures is one in which the functional oxide film can be epitaxially grown directly on silicon. Such direct integration is, however, complicated by the high reactivity of silicon with oxygen and the disruption of epitaxy that results from the presence of the resulting amorphous silicon oxide layer at the surface of silicon wafers. An epitaxial buffer layer is, therefore, a general prerequisite to the growth of epitaxial functional oxides on silicon having high structural perfection. An additional challenge is the large difference in the thermal expansion coefficients between silicon and these functional oxides; the ratio of thermal expansion coefficients is about a factor of three between room temperature and growth temperature.

To fabricate epitaxial structures in which the properties of the underlying silicon and the overlying film both achieve their full potential, control of the silicon-oxide interface is critical. Fundamental considerations that must be taken into account in the selection of appropriate epitaxial buffer layers include chemical and structural compatibilities.[17] For the case of silicon, a comprehensive analysis of its thermodynamics stability in contact with binary oxides has been performed.[18] Reactions leading to the formation of interfacial silicide, silicate, or SiO_2 layers have been reported when these oxides are exposed to high temperatures during device processing.[19] A large number of oxides have been grown epitaxially on Si (100) or Si (111). The list includes $SrTiO_3$, SrO, BaO, $BaTiO_3$, CeO_2, ZrO_2, YSZ, Y_2O_3, Sc_2O_3, Pr_2O_3, Gd_2O_3, $La(Y)_2O_3$, and γ-Al_2O_3 as reviewed by Reiner *et al.*[20] In terms of structural compatibility, few oxides are well lattice matched to (100) Si. The lattice match of the small number of oxides with the perovskite structure that has been epitaxially integrated with (100) Si using a thin (as thin as a single monolayer (ML)) binary oxide buffer layer is shown in Fig. 1. These include $CaTiO_3$,[21,22] $SrTiO_3$,[21–25] $BaTiO_3$,[21,22,26,27] $SrZrO_3$,[28] and $SrHfO_3$.[29,30] The latter two, $SrZrO_3$ and $SrHfO_3$, with pseudocubic lattice constants of 4.101 Å and 4.070 Å at room temperature, respectively, lie off the top of Fig. 1.

Among these materials, $SrTiO_3$ (cubic cell with c = 3.905 Å) has been the most widely pursued perovskite buffer layer, but due to the large lattice mismatch with Si (1.7%), $SrTiO_3$ begins to relax for thickness beyond a few nanometers in thickness, drastically degrading the crystalline quality of the $SrTiO_3$ buffer layer.[31] $CaTiO_3$ (orthorhombic unit cell with a = 5.3789 Å, b = 5.4361 Å, and c = 7.6388 Å at room temperature),[32] yielding a pseudocubic lattice constant of 3.822 Å, has an excellent lattice match to (100) Si (cubic cell with c = 5.431 Å) as is readily apparent from Fig. 1. This makes it an obvious candidate as a buffer layer. Thick, commensurate $CaTiO_3$ layers on (100) Si should be in principle realizable. The excellent lattice match should greatly reduce the in-plane and out-of-plane rotation variation achievable in epitaxial perovskite layers on (100) Si. Although

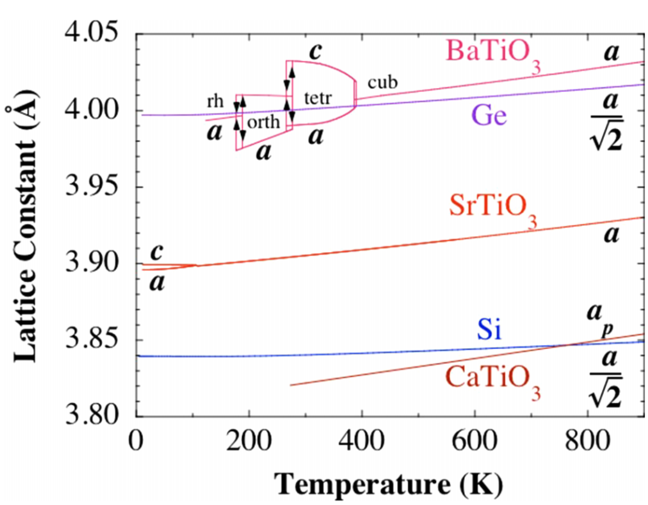

FIG. 1. Temperature dependence of the lattice constants of the perovskites $CaTiO_3$, $SrTiO_3$, and $BaTiO_3$ compared to the lattice parameter of silicon. The lattice parameters of silicon (and germanium) are divided by $\sqrt{2}$ as is relevant for the in-plane epitaxial alignment of $(100)_p$ $A$$TiO_3$/(100) Si with $[011]_p$ $A$$TiO_3$ ∥ [001] Si, where the subscript p denotes pseudocubic indices. The pseudocubic lattice parameter a_p of $CaTiO_3$ is plotted.

reported,[21,22] the potential of $CaTiO_3$ as a buffer layer to transition from (100) Si to functional oxides with the perovskite structure has been largely ignored.

In this paper, we show that the mineral perovskite, $CaTiO_3$, can be used as a buffer layer in the epitaxial transition from (100) Si substrates to perovskite functional oxides, such as $La_{0.7}Sr_{0.3}MnO_3$. We demonstrate here that $La_{0.7}Sr_{0.3}MnO_3$ films deposited on $CaTiO_3$/Si indeed showed enhanced electrical properties (e.g., lower electrical resistivity and $1/f$ noise, and high temperature of the metal-to-insulator transition) as well as enhanced magnetic properties (higher Curie temperature) compared to other epitaxial $La_{0.7}Sr_{0.3}MnO_3$ thin films deposited on buffered silicon substrates.[33–39]

We grew epitaxial $CaTiO_3$ thin films on (100) Si by reactive molecular-beam epitaxy (MBE). The native SiO_2 layer was removed from the (100) Si substrate using a strontium assisted process.[40] Two monolayers of strontium metal (corresponding to 1.2×10^{15} atoms/cm^2) were deposited at a substrate temperature of T = 600 °C. Then, the substrate temperature was increased to T = 800 °C. At this temperature, the silicon dioxide layer was removed by the formation and evaporation of SiO_x,[40] and a single crystalline reflection high-energy electron diffraction (RHEED) pattern with a double-domain 2×1 (100) Si reconstruction was observed.

$CaTiO_3$ films were grown using a codeposition technique in a manner analogous to the leading technique for producing the highest quality $SrTiO_3$/Si films.[25,31] Calcium was evaporated from an effusion cell and titanium from a Ti-Ball™ sublimation source.[41] The fluxes of the constituent elements, calcium and titanium, were measured using a quartz crystal monitor and typical values for each element were around 1×10^{13} atoms/cm^2 s. A substrate temperature of 330 °C was used to grow the first 2.5 MLs at a background partial pressure of molecular oxygen of 7×10^{-9} Torr. Figure 2(a) shows the RHEED pattern after the deposition of 2.5 MLs of $CaTiO_3$. To improve the crystallinity of the films, the oxygen valve was closed and the substrate temperature was increased, in

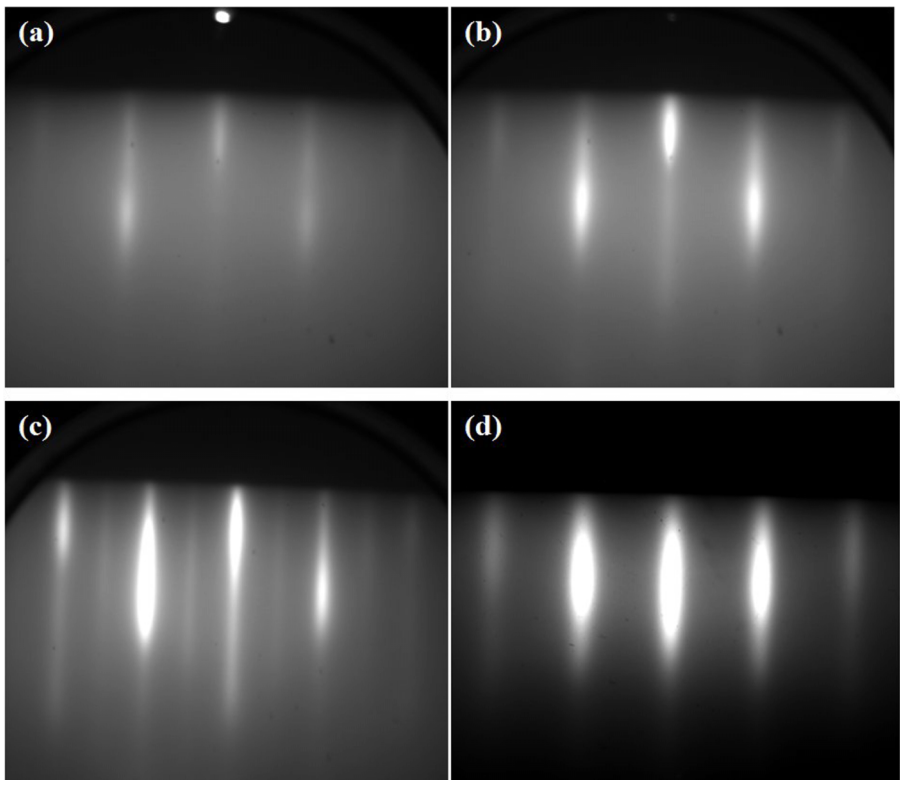

FIG. 2. RHEED patterns at various times during the growth of a 50 nm $La_{0.7}Sr_{0.3}MnO_3$/20 nm $CaTiO_3$/Si heterostructure. (a) After the growth of 2.5 MLs of $CaTiO_3$ at T = 330 °C viewed along the $[100]_P$ azimuth of $CaTiO_3$. (b) After the growth of 2.5 MLs of $CaTiO_3$ after annealing in vacuum at T = 600 °C viewed along the $[100]_P$ azimuth of $CaTiO_3$. (c) After the growth of 20 nm of $CaTiO_3$ viewed along the $[100]_P$ azimuth of $CaTiO_3$. (d) After the growth of 50 nm of $La_{0.7}Sr_{0.3}MnO_3$ completing the heterostructure viewed along the $[100]_P$ azimuth of $La_{0.7}Sr_{0.3}MnO_3$.

vacuum, to 580 °C for 15 min (as shown in Fig. 2(b)). Next, the sample was cooled down to 330 °C to grow a second 2.5 MLs of $CaTiO_3$ under the same growth conditions as the first 2.5 MLs. Again the sample was annealed in vacuum at T = 580 °C for 8 min. At this temperature, the calcium, titanium, and oxygen shutters were opened simultaneously, and with the oxygen background pressure at 1×10^{-7} Torr, the thickness of the epitaxial $CaTiO_3$ layer was grown to 20-40 nm. Figure 2(c) shows the RHEED pattern at the end of the growth of the 20-nm thick $CaTiO_3$ layer. Rutherford backscattering spectrometry/channeling (RBS/C) utilizing He^+ ions with an energy of 1.4 MeV was applied to investigate the composition and crystalline quality of the films. The computer software RUMP was employed to analyze the RBS data.[42] The films have a Ca:Ti composition ratio of 1.05 ± 0.05. A RBS/C minimum yield χ_{min} = 12% was observed.

Following the growth of the $CaTiO_3$ film, 50 nm of $La_{0.7}Sr_{0.3}MnO_3$ was deposited on it. The $La_{0.7}Sr_{0.3}MnO_3$ film was grown at a substrate temperature of 670 °C by codeposition in a distilled ozone background pressure of 5×10^{-7} Torr.[43] The RHEED pattern at the completion of the 50-nm thick $La_{0.7}Sr_{0.3}MnO_3$ layer completing the $La_{0.7}Sr_{0.3}MnO_3/CaTiO_3/Si$ heterostructure is shown in Fig. 2(d).

Film structural properties and morphology were investigated by X-ray diffraction (XRD) and by atomic force microscopy (AFM) in tapping mode (Digital Instruments—Nanoscope III). Cross sectional transmission electron microscopy (TEM) specimens were prepared by mechanical grinding and polishing, followed by argon ion milling (Gatan model 691 Precision Ion Polishing System) to electron transparency. The samples were examined using a JEOL 3011 high resolution TEM, operated at 300 kV.

In Fig. 3(a), a θ-2θ x-ray diffraction scan of the $La_{0.7}Sr_{0.3}MnO_3/CaTiO_3/Si$ heterostructure is shown. The labels indicate the $h00_p$ series of $CaTiO_3$ and $La_{0.7}Sr_{0.3}MnO_3$ peaks. As expected, the $La_{0.7}Sr_{0.3}MnO_3$ film grows under compressive strain which results in a larger out-of-plane lattice constant c = 3.905 Å compared to bulk $La_{0.7}Sr_{0.3}MnO_3$, which has a pseudocubic lattice spacing of 3.876 Å. Figure 3(b) shows the rocking curve in ω of the 200_p reflections of the $CaTiO_3$ and $La_{0.7}Sr_{0.3}MnO_3$ layers of the heterostructure. They have full width at half maximum (FWHM) of 0.67° and 0.71°, respectively. The epitaxy was verified by off-axis ϕ scans of the 110_p $CaTiO_3$ peak as shown in Fig. 3(b). The peak has a FWHM of 0.86° in ϕ. A smooth surface with a root mean square (RMS) roughness of 0.5 nm was measured over a 1 μm × 1 μm region by AFM (see Fig. 4). This is the lowest value reported for manganite films of comparable thickness grown on silicon substrates.[39,44–47]

The microstructure of the $La_{0.7}Sr_{0.3}MnO_3/CaTiO_3/Si$ epitaxial heterostructure was studied by TEM. Figure 5(a) shows the overall microstructure of the specimen, including an amorphous SiO_x layer, which formed *in situ* by the diffusion of oxygen through the growing epitaxial film and oxidation of the underlying silicon substrate during the film growth. The formation of SiO_x layers during growth is common in epitaxial oxide on silicon systems when the oxygen partial pressure is high and at the same time, the silicon substrate is hot.[48,49] The out-of-plane linear defects evident in Fig. 5(a) are rotation domain boundaries, common to $CaTiO_3$. A typical region of the $La_{0.7}Sr_{0.3}MnO_3/CaTiO_3$ interface, exhibiting good epitaxy between the two layers, is shown in Fig. 5(b). A selected-area electron diffraction (SAED) pattern, taken from both film layers simultaneously, is shown in Fig. 5(c). No spot-splitting is evident, consistent with good epitaxy between the two layers.

We have performed electrical and magnetic measurements on this same sample. Electrical resistivity measurements as a function of temperature were performed on unpatterned films by the standard four-probe technique. Magnetization was measured by a superconducting quantum interference device (SQUID) magnetometer. Figure 6(b) reports the magnetization as a function of temperature in a field of 0.01 T. The zero-field-cooled (not shown) and field-cooled magnetizations have been measured. The curve has been fitted by a theoretical standard static Brillouin magnetization function. The $La_{0.7}Sr_{0.3}MnO_3$ shows a rapid increase of the magnetic moment below the Curie temperature T_C = 360 K, and the saturated magnetization value at low temperature is 3.5 μ_B/Mn. These values are similar to the values of bulk $La_{0.7}Sr_{0.3}MnO_3$[50] and the highest reported for thin films grown on silicon substrates.[44,47,51] The metal-insulator transition temperature is consistent with the magnetic properties. The temperature dependence of the electrical resistivity is shown in Fig. 6(a). The film shows a metal-insulator transition temperature, T_{MI}, higher than 400 K. This

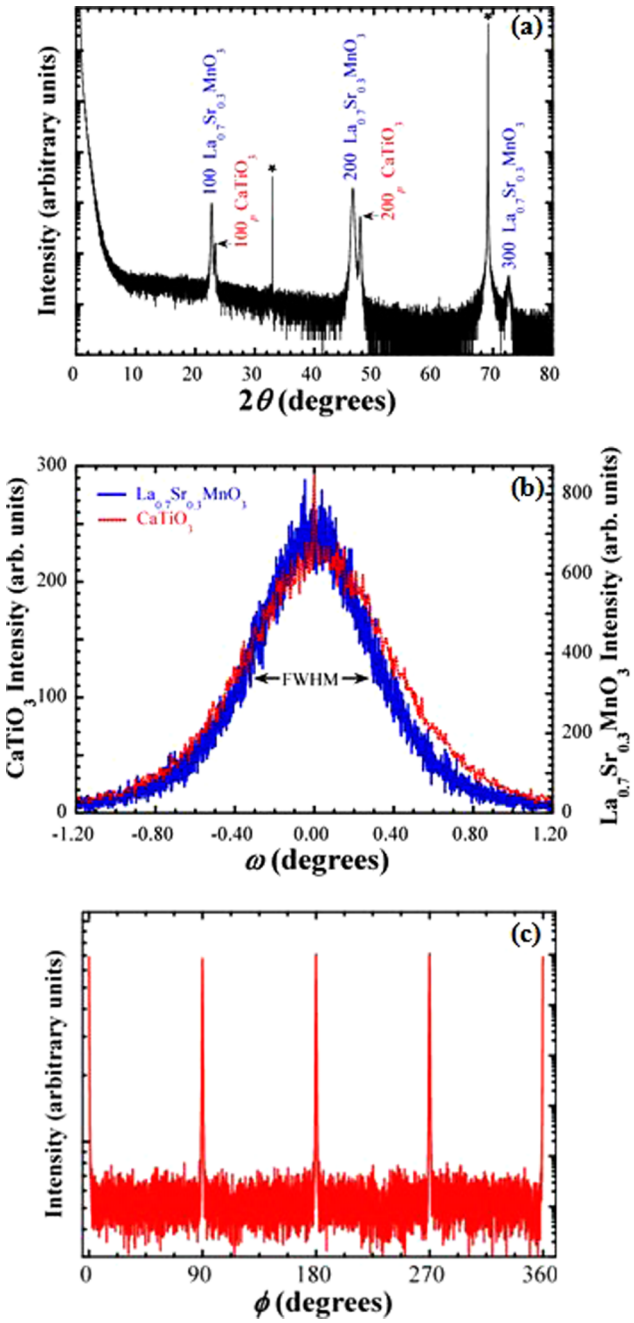

FIG. 3. (a) θ-2θ XRD scans of the same $La_{0.7}Sr_{0.3}MnO_3/CaTiO_3/Si$ heterostructure whose RHEED patterns are shown in Fig. 2. (b) Rocking curves in ω of the 200_p reflection of the $La_{0.7}Sr_{0.3}MnO_3$ and the 200_p reflection of $CaTiO_3$ of the same heterostructure. (c) ϕ-scan of the 110_p $CaTiO_3$ peak.

is the highest value reported for $La_{0.7}Sr_{0.3}MnO_3$ grown with or without a buffer layer on silicon substrates.[36–38,44,47,51–55] Moreover, the electrical resistivity value at 300 K is 1.5 mΩ cm, which is quite similar to bulk $La_{0.7}Sr_{0.3}MnO_3$,[56] and lower by a factor 2 compared to what we have obtained in the $La_{0.7}Sr_{0.3}MnO_3$ films of comparable thickness deposited on $SrTiO_3/Si$ by the same MBE technique. We also measured the electrical resistivity of a single $CaTiO_3$ layer on (100) Si substrate to rule out the effect of the oxygen content on the physical properties of $CaTiO_3$.[21,22] The film was grown under the same conditions as that used for the $CaTiO_3$ part of our $La_{0.7}Sr_{0.3}MnO_3/CaTiO_3/Si$

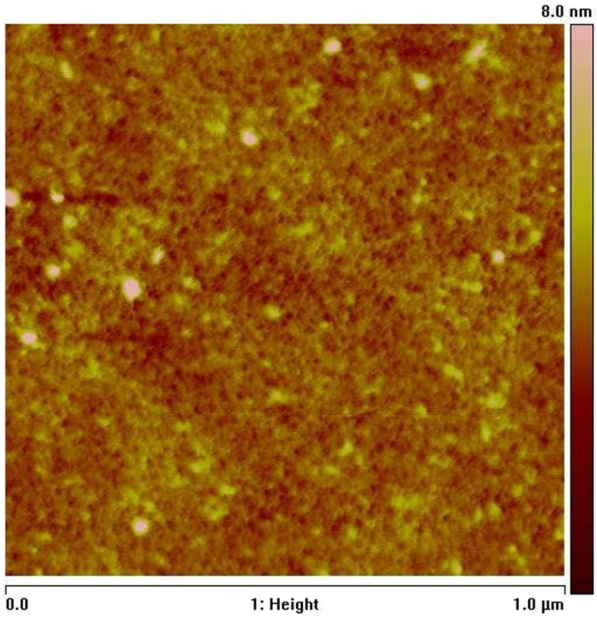

FIG. 4. 1 μm × 1 μm AFM images in tapping mode of the same $La_{0.7}Sr_{0.3}MnO_3/CaTiO_3/Si$ heterostructure in Figs. 2 and 3.

heterostructures. The inset of Fig. 6(a) shows the electrical resistance as a function of temperature for a bare 20-nm thick $CaTiO_3$ film on a (100) Si substrate. Insulating behavior over the whole temperature range is observed. This leads us to conclude that both the electrical and magnetic properties are enhanced compared to those reported in high epitaxial quality $La_{0.7}Sr_{0.3}MnO_3$ films deposited on $SrTiO_3$ buffered Si substrates,[39] where T_{MI} and T_C values were 350 K and 330 K, respectively. We ascribe the enhancement of these properties to the fact that the $La_{0.7}Sr_{0.3}MnO_3$ cell is under compressive in-plane strain on $CaTiO_3$/Si as predicted by Millis *et al.*[57] and also experimentally observed in Ref. 43.

Electrical low-frequency noise measurements were performed at 300 K in the same way as previously described.[39,58,59] The $La_{0.7}Sr_{0.3}MnO_3/CaTiO_3$/Si thin film was patterned by UV photolithography and argon ion etching to form a 50 μm wide and 150 μm long strip, which includes two gold pads for supplying the current and two gold pads at which the voltage was measured in a four-probe geometry. Figure 7 presents the voltage noise spectral density measured at various

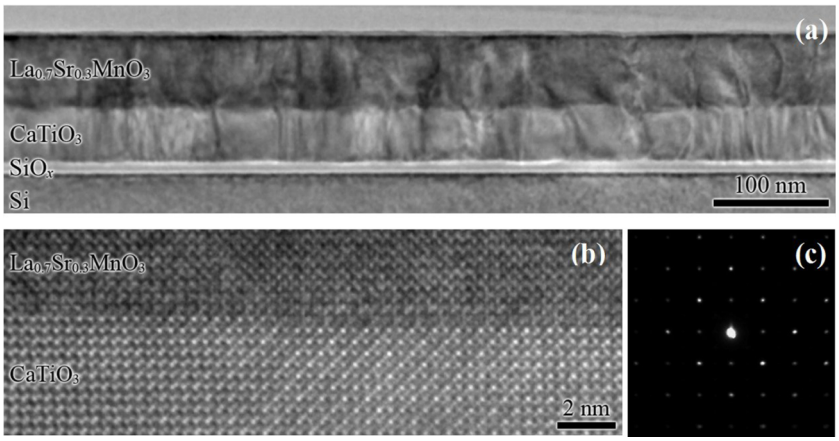

FIG. 5. TEM micrographs of a $La_{0.7}Sr_{0.3}MnO_3/CaTiO_3$/Si heterostructure showing (a) a lower magnification image of the entire heterostructure, (b) a close-up of the $La_{0.7}Sr_{0.3}MnO_3/CaTiO_3$ interface, and (c) a SAED pattern from both the $La_{0.7}Sr_{0.3}MnO_3$ and $CaTiO_3$ layers.

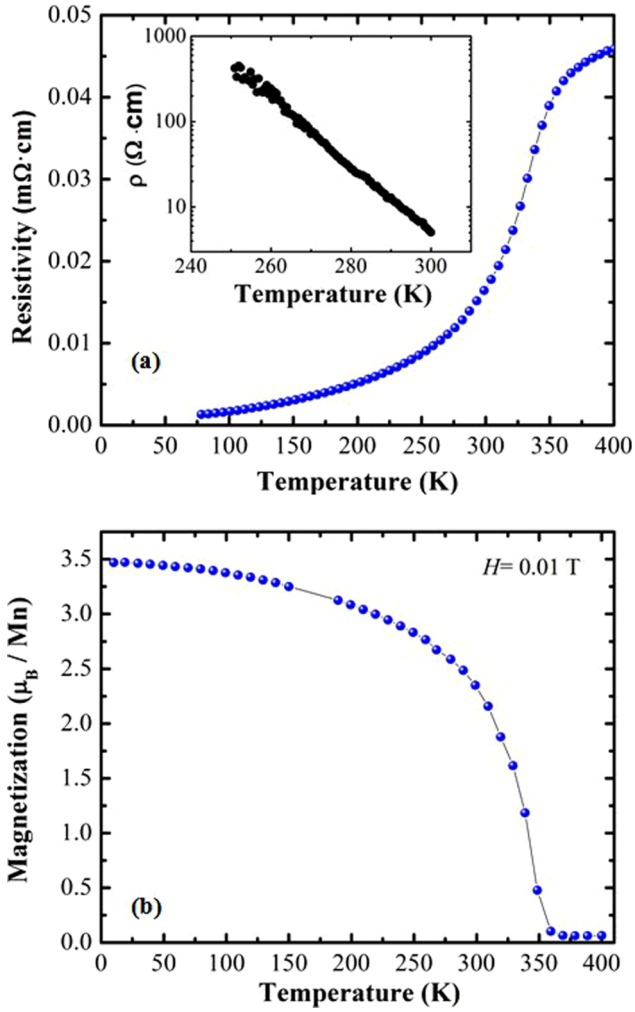

FIG. 6. (a) Resistivity vs. temperature of $La_{0.7}Sr_{0.3}MnO_3$ grown on $CaTiO_3$/Si. The inset shows the resistivity of a 20-nm thick $CaTiO_3$ buffer layer on silicon. (b) Temperature dependence of the magnetization ($M(T)$) in a magnetic field of 0.01 T of the same heterostructure shown in Figs. 2–4.

bias currents. We can clearly observe both Johnson (or thermal) noise at high frequency and $1/f$ (or flicker) noise at low frequency. In contrast to Johnson noise, which depends neither on bias current nor on frequency, the latter gives a frequency and bias current dependent contribution to noise, which gives an indication of the material quality.[60] This $1/f$ noise is usually described by the Hooge empirical relation, which does not have any physical basis, but has been shown to agree well with experimental observations for homogeneous samples. This relation is given by the following general formula:[61]

$$\frac{S_V}{V^2} = \frac{\alpha_H}{n} \times \frac{1}{\Omega \times f}, \tag{1}$$

where S_V is the voltage noise spectral density ($V^2\ Hz^{-1}$), V is the sample voltage (V), α_H is the Hooge parameter (dimensionless), n is the charge carrier density (m^{-3}), Ω is the sample volume (m^3), and f is the measuring frequency (Hz). It is very useful to compare the $1/f$ noise magnitude in different materials independent of the sample volume and the bias conditions. In order to estimate the voltage noise spectral density of the material, the noise of the electronic readout and the noise of the voltage contacts were removed. As presented in the inset of Fig. 7, the quadratic dependence of the voltage noise spectral density at 1 Hz and at 300 K versus the sample voltage was verified

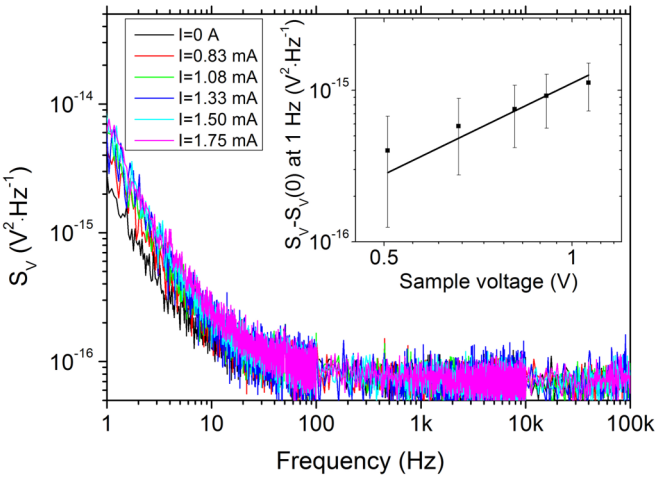

FIG. 7. Voltage noise spectral density plots of a 50 μm wide by 150 μm long strip patterned in the same $La_{0.7}Sr_{0.3}MnO_3$ film of Figs. 2–4 grown on $CaTiO_3$/Si measured at various bias currents. The inset shows the voltage noise spectral density at 1 Hz versus the sample voltage.

within experimental error bars as expected from Eq. (1), thus enabling a correct estimation of α_H/n values. The normalized Hooge parameters α_H/n was then measured to be $(4.2 \pm 0.6) \times 10^{-31}$ m^3 at 300 K, which is about two times lower than the one measured in $La_{0.7}Sr_{0.3}MnO_3$ films of comparable thickness deposited on $SrTiO_3$/Si with α_H/n values of $(9.8 \pm 0.6) \times 10^{-31}$ m^3 at 300 K and only two times higher than the one measured in $La_{0.7}Sr_{0.3}MnO_3$ films of comparable thickness deposited on $SrTiO_3$ single crystal substrates with α_H/n values of $(2.47 \pm 0.6) \times 10^{-31}$ m^3.[39,58,59]

In conclusion, we have shown the promise of epitaxial $(100)_p$-oriented $CaTiO_3$ as a buffer layer for the integration of functional oxides having the perovskite structure with silicon. Specifically, we have grown high-quality epitaxial $La_{0.7}Sr_{0.3}MnO_3$ films on $CaTiO_3$/Si. Both the Curie and the metal-to-transition temperatures are the highest reported values for $La_{0.7}Sr_{0.3}MnO_3$ thin films deposited on buffered silicon substrates. The corresponding electrical resistivity and the $1/f$ noise level are decreased by a factor of two compared to those measured in high-quality epitaxial $La_{0.7}Sr_{0.3}MnO_3$ thin films of comparable thickness deposited on $SrTiO_3$/Si. These films exhibit magnetic and electrical properties comparable with bulk $La_{0.7}Sr_{0.3}MnO_3$, making them of interest for room temperature applications on silicon substrates.

We gratefully acknowledge the financial support of Intel and the National Science Foundation through the MRSEC program (Grant Nos. DMR-1120296 and DMR-1420620), and Grant Nos. ECCS-0708759 and DMR-0315633. This work was performed in part at the Cornell NanoScale Facility, a member of the National Nanotechnology Infrastructure Network, which is supported by the National Science Foundation (Grant ECCS-0335765).

[1] *Nanoelectronics and Information Technology: Advanced Materials and Novel Devices*, 2nd ed., edited by R. Waser (Wiley-VCH, Weinheim, 2005).
[2] M. Bibes and A. Barthelemy, IEEE Trans. Electron Devices **54**, 1003 (2007).
[3] D. G. Schlom, L. Q. Chen, X. Q. Pan, A. Schmehl, and M. A. Zurbuchen, J. Am. Ceram. Soc. **91**, 2429 (2008).
[4] R. Ramesh and D. G. Schlom, MRS Bull. **33**, 1006 (2008).
[5] J. Heber, Nature **459**, 28 (2009).
[6] S. D. Ha and S. Ramanathan, J. Appl. Phys. **110**, 071101 (2011).
[7] F. Miletto Granozio, G. Koster, and G. Rijnders, MRS Bull. **38**, 1017 (2013).
[8] H. Akinaga, Jpn. J. Appl. Phys., Part 1 **52**, 100001 (2013).
[9] M. D. Nguyen, H. Nazeer, K. Karakaya, S. V. Pham, R. Steenwelle, M. Dekkers, L. Abelmann, D. H. A. Blank, and G. Rijnders, J. Micromech. Microeng. **20**, 085022 (2010).
[10] D. Isarakorn, A. Sambri, P. Janphuang, D. Briand, S. Gariglio, J.-M. Triscone, F. Guy, J. W. Reiner, C. H. Ahn, and N. F. de Rooij, J. Micromech. Microeng. **20**, 055008 (2010).
[11] S. Trolier-McKinstry and P. Muralt, J. Electroceram. **12**(1-2), 7 (2004).

[12] S. H. Baek, J. Park, D. M. Kim, V. A. Aksyuk, R. R. Das, S. D. Bu, D. A. Felker, J. Lettieri, V. Vaithyanathan, S. S. N. Bharadwaja, N. Bassiri-Gharb, Y. B. Chen, H. P. Sun, C. M. Folkman, H. W. Jang, D. J. Kreft, S. K. Streiffer, R. Ramesh, X. Q. Pan, S. Trolier-McKinstry, D. G. Schlom, M. S. Rzchowski, R. H. Blick, and C. B. Eom, Science **334**, 958 (2011).
[13] H. Colder, B. Domengès, C. Jorel, P. Marie, M. Boisserie, S. Guillon, L. Nicu, A. Galdi, and L. Méchin, J. Appl. Phys. **115**, 053506 (2014).
[14] S. Liu, B. Guillet, A. Aryan, C. Adamo, C. Fur, J.-M. Routoure, F. Lemarié, D. G. Schlom, and L. Méchin, Microelectron. Eng. **111**, 101 (2013).
[15] M. Madou, *Fundamentals of Microfabrication and Nanotechnology*, 3rd ed. (CRC Press, Boca Raton, 2011).
[16] J. Baborowski, J. Electroceram. **12**, 33 (2004).
[17] J. M. Phillips, J. Appl. Phys. **79**, 1829 (1996).
[18] K. J. Hubbard and D. G. Schlom, J. Mater. Res. **11**, 2757 (1996).
[19] S. Stemmer, J. Vac. Sci. Technol. B **22**, 791 (2004).
[20] J. W. Reiner, A. M. Kolpak, Y. Segal, K. F. Garity, S. Ismail-Beigi, H. Ahn, and F. J. Walker, Adv. Mater. **22**, 2919 (2010).
[21] F. J. Walker and R. A. McKee, *High Dielectric Constant Materials: VLSI MOSFET Applications*, edited by H. R. Huff and D. C. Gilmer (Springer, Berlin, 2005), pp. 607–637.
[22] R. A. McKee and F. J. Walker, U.S. patent 5,830,270 (3 November, 1998).
[23] G. Niu, G. Saint-Girons, B. Vilquin, G. Delhaye, J.-L. Maurice, C. Botella, Y. Robach, and G. Hollinger, Appl. Phys. Lett. **95**, 062902 (2009).
[24] R. A. McKee, F. J. Walker, and M. Chisholm, Phys. Rev. Lett. **81**, 3014 (1998).
[25] H. Li, X. Hu, Y. Wei, Z. Yu, X. Zhang, R. Droopad, A. A. Demkov, J. Edwards, Jr., K. Moore, W. Ooms, J. Kulik, and P. Fejes, J. Appl. Phys. **93**, 4521 (2003).
[26] R. A. McKee, F. J. Walker, J. R. Conner, E. D. Specht, and D. E. Zelmon, Appl. Phys. Lett. **59**, 782 (1991).
[27] V. Vaithyanathan, J. Lettieri, W. Tian, A. Kochhar, H. Ma, A. Sharan, A. Vasudevarao, V. Gopalan, Y. Li, L. Q. Chen, P. Zschack, J. C. Woicik, J. Levy, and D. G. Schlom, J. Appl. Phys. **100**, 024108 (2006).
[28] D. Halley, G. Norga, A. Guiller, J. Fompeyrine, J. P. Locquet, U. Drechsler, H. Siegwart, and C. Rossel, J. Appl. Phys. **94**, 6607 (2003).
[29] C. Rossel, B. Mereu, C. Marchiori, D. Caimi, M. Sousa, A. Guiller, H. Siegwart, R. Germann, J. P. Locquet, J. Fompeyrine, D. J. Webb, C. Dieker, and J. W. Seo, Appl. Phys. Lett. **89**, 053506 (2006).
[30] M. Sousa, C. Rossel, C. Marchiori, H. Siegwart, D. Caimi, J. P. Locquet, D. J. Webb, R. Germann, J. Fompeyrine, K. Babich, J. W. Seo, and C. Dieker, J. Appl. Phys. **102**, 104103 (2007).
[31] M. P. Warusawithana, C. Cen, C. R. Sleasman, J. C. Woicik, Y. L. Li, L. F. Kourkoutis, J. A. Klug, H. Li, P. Ryan, L. P. Wang, M. Bedzyk, D. A. Muller, L. Q. Chen, J. Levy, and D. G. Schlom, Science **324**, 367 (2009).
[32] R. Ali and M. Yashima, J. Solid State Chem. **178**, 2867 (2005).
[33] Z. Trajanovic, C. Kwon, M. C. Robson, K.-C. Kim, M. Rajeswari, R. Ramesh, T. Venkatesan, S. E. Lofland, S. M. Bhagat, and D. Fork, Appl. Phys. Lett. **69**, 1005 (1996).
[34] I. Bergenti, V. Dediu, E. Arisi, M. Cavallini, F. Biscarini, C. Taliani, M. P. de Jong, C. L. Dennis, J. F. Gregg, M. Solzi, and M. Natali, J. Magn. Magn. Mater. **312**, 453 (2007).
[35] J.-H. Kim, S. I. Khartsev, and A. M. Grishin, Appl. Phys. Lett. **82**, 4295 (2003).
[36] L. Méchin, P. Perna, C. Barone, J.-M. Routoure, and Ch. Simon, Mater. Sci. Eng. B **144**, 73 (2007).
[37] A. K. Pradhan, D. Hunter, T. Williams, B. Lasley-Hunter, R. Bah, H. Mustafa, R. Rakhimov, J. Zhang, D. J. Sellmyer, E. E. Carpenter, D. R. Sahu, and J.-L. Huang, J. Appl. Phys. **103**, 023914 (2008).
[38] P. Perna, L. Méchin, M. P. Chauvat, P. Ruterana, Ch. Simon, and U. Scotti di Uccio, J. Phys.: Condens. Matter **21**, 306005 (2009).
[39] L. Méchin, C. Adamo, S. Wu, B. Guillet, S. Lebargy, C. Fur, J.-M. Routoure, S. Mercone, M. Belmeguenai, and D. G. Schlom, Phys. Status Solidi A **209**, 1090 (2012).
[40] Y. Wei, X. Hu, Y. Liang, D. C. Jordan, B. Craigo, R. Droopad, Z. Yu, A. Demkov, J. L. Edwards, Jr., K. Moore, and W. J. Ooms, *Silicon Materials-Processing Characterization and Reliability*, edited by J. Veteran, D. L. O'Meara, and V. Misra (Materials Research Society, Warrendale, 2002), Vol. 716, pp. B3.4.1–B3.4.6.
[41] C. D. Theis and D. G. Schlom, J. Vac. Sci. Technol., A **14**, 2677 (1996).
[42] L. R. Doolittle, Nucl. Instrum. Methods Phys. Res., Sect. B **9**, 344 (1985).
[43] C. Adamo, X. Ke, H. Q. Wang, H. L. Xin, T. Heeg, M. E. Hawley, W. Zander, J. Schubert, P. Schiffer, D. A. Muller, L. Maritato, and D. G. Schlom, Appl. Phys. Lett. **95**, 112504 (2009).
[44] J. Y. Gu, C. Kwon, M. C. Robson, Z. Trajanovic, K. Ghosh, R. P. Sharma, R. Shreekala, M. Rajeswari, T. Venkatesan, R. Ramesh, and T. W. Noh, Appl. Phys. Lett. **70**, 1763 (1997).
[45] I.-B. Shim, C.-S. Kim, K.-T. Park, and Y.-J. Oh, J. Magn. Magn. Mater. **226**, 1672 (2001).
[46] K. Pradhan, S. Mohanty, K. Zhang, J. B. Dadson, E. M. Jackson, D. Hunter, R. R. Rakhimov, and G. B. Loutts, Appl. Phys. Lett. **86**, 012503 (2005).
[47] D. Hunter, J. B. Dadson, K. Zhang, B. Lasley, K. Lord, S. Mohanty, T. M. Williams, R. R. Rakhimov, A. K. Pradhan, J. Zhang, and D. J. Sellmyer, J. Appl. Phys. **99**, 08Q307 (2006).
[48] Th. Matthée, J. Wecker, H. Behner, G. Friedl, O. Eibl, and K. Samwer, Appl. Phys. Lett. **61**, 1240 (1992).
[49] T. Inoue, T. Ohsuna, Y. Obara, Y. Yamamoto, M. Sato, and Y. Sakurai, Jpn. J. Appl. Phys., Part 1 **32**, 1765 (1993).
[50] K. Hirota, N. Kaneko, and Y. Endoh, J. Phys. Soc. Jpn. **65**, 3736 (1996).
[51] A. Tiwari, A. Chug, C. Jin, D. Kumar, and J. Narayan, Solid State Commun. **121**, 679 (2002).
[52] Y. S. Cho, J. S. Hwang-Bo, Y. Hee kim, S.-I. Park, S. Won Lee, and C. S. Kim, J. Magn. Magn. Mater. **226**, 754 (2001).
[53] S. M. Liua, X. B. Zhua, J. Yanga, B. C. Zhaoa, Z. G. Shenga, W. H. Songa, J. M. Daia, and Y. P. Sun, Physica B **353**, 238 (2004).
[54] D. R. Sahu, D. K. Mishra, J.-L. Huang, and B. K. Roul, Physica B **396**, 75 (2007).
[55] Y.-M. Kang, A. N. Ulyanov, G.-M. Shin, S.-Y. Lee, D.-G. Yoo, and S.-I. Yoo, J. Appl. Phys. **105**, 07D711 (2009).

[56] A. Urushibara, Y. Mortomo, T. Arima, A. Asamitsu, G. Kido, and Y. Tokura, Phys. Rev. B **51**, 14103 (1995).
[57] A. J. Millis, T. Darling, and A. Migliori, J. Appl. Phys. **83**, 1588 (1998).
[58] L. Méchin, J.-M. Routoure, S. Mercone, F. Yang, S. Flament, and R. A. Chakalov, J. Appl. Phys. **103**, 083709 (2008).
[59] L. Méchin, S. Wu, B. Guillet, P. Perna, C. Fur, S. Lebargy, C. Adamo, D. G. Schlom, and J. M. Routoure, J. Phys. D: Appl. Phys. **46**, 202001 (2013).
[60] F. N. Hooge, T. G. M. Kleinpenning, and L. K. J. Vandamme, Rep. Prog. Phys. **44**, 481 (1981).
[61] F. N. Hooge, Phys. Lett. A **29**, 139 (1969).